2003-01-1477

Examination of Some Vibration Isolator Models and Their Effects on Vibration and Structure-borne Noise Transmission

Seungbo Kim and Rajendra Singh
The Ohio State University

ABSTRACT

A vibration isolator or mount is often modeled by the Voigt model describing uni-axial (longitudinal) motion with frequency-invariant parameters. However, wave effects due to the mass distribution within the isolator are observed as the frequency is increased. Further, flexural stiffness components play an important role, leading to off-axis and coupling effects. Thus, the simplified mount models could lead to erroneous predictions of the dynamic behavior of an overall system such as automotive powertrain or chassis mounting systems. This article compares various approximate isolator models using a multi-dimensional mobility model that is based on the continuous system theory. Harmonic force and moment excitations are separately applied to a rigid body source to investigate the multi-dimensional vibratory behavior. Analysis is however limited to a linear time-invariant system and the mobility synthesis method is utilized to predict the frequency domain behavior. Alternate receiver models, such as infinite and finite plates, are employed to examine the asymptotic and resonant behaviors of the power-based isolation measures. Finally, an inverted 'L' plate receiver is selected to represent a simplified vehicle body structure and sound radiated from this receiver is computed to assess the structure-borne noise transmitted through mounts. The roles and effects of coupling terms, frequency dependency and discrete element modeling of stiffnesses on vibration and sound isolation measures are identified over a broad range of frequencies.

INTRODUCTION

An isolator must be properly modeled to predict the accurate dynamic response of a system. In many cases, an isolator is characterized by a frequency-invariant discrete element in the uni-axial (compressional) direction [1]. However, the rotational stiffness could be a significant contributor to the vibration transmission [2] and hence some studies have included the rotational elements of isolators [2, 3]. Yet most researchers ignore the coupling stiffnesses in flexural motions [2] although the rotational components must be handled by a coupled formulation with lateral components in flexure [4]. The role and significance of such coupling terms on the isolator stiffnesses have not been investigated. Furthermore, it is well known that wave effects occur within the isolators at higher frequencies and therefore the isolator model must describe the frequency-dependent characteristics as frequency increases [5]. We recently proposed a new method that can characterize multi-dimensional stiffnesses of an isolator over a broad frequency range [6]. The use of spectrally-varying stiffnesses characterized by such schemes may enhance the prediction of system response. Yet, the frequency-dependent stiffness model, which incorporates inertial or standing waves within the isolator, is incomplete since forces are assumed to be identical through the stiffness element unlike a real-life mount. Complete description of a mount requires both cross-point and driving point stiffnesses. Recently, isolator models based on the continuous system theory have been employed to describe the multi-dimensional vibration transmission problems [3, 6, 7]. However, an accurate identification of the driving point stiffnesses is not straightforward for most cases since results are extremely sensitive to associated experimental fixturing.

Given the lack of comprehensive isolator model, one may attempt to describe a mount with an approximate model. Nonetheless, discrepancies between the spectrally-varying stiffness and continuous models have not drawn much attention. This article examines the effects of such isolator modeling approximations on vibration and structure-borne noise transmission. We will also compare predictions from approximate models with the ones from a mobility-based model. Problem is defined in Figure 1 via an isolation system with a multi-dimensional isolator and two alternate compliant receivers. Figure 1 also illustrates vibration components transmitted through a multi-dimensional isolator.

Continuous system models of an isolator, which are the Timoshenko beam (in the flexural x and θ directions) and the longitudinal (y) wave equation formulations, have been developed in an earlier article [3] and these are utilized here. Other formulations that we developed in our prior studies are also employed in this article such as the mobility synthesis formulation for predicting the overall system behavior [6] and structure-borne noise measures [8].

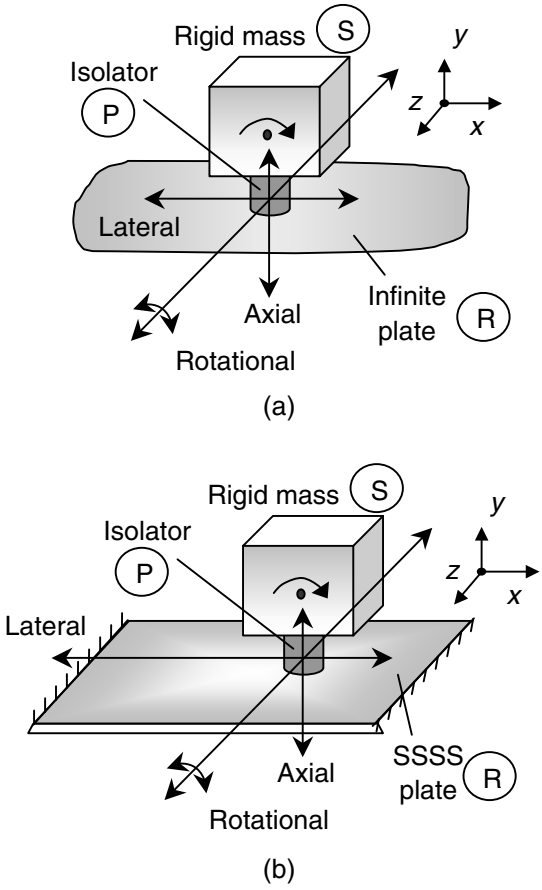

Figure 1. Configuration of the vibration isolation system. (a) System with an infinite plate receiver; (b) system with a finite plate receiver of all boundaries simply supported (SSSS). Here, S implies a simply supported edge.

Chief objectives of this study are. 1. Examine the approximate stiffness models of a multi-dimensional isolator along with actual stiffness components modeled by the continuous system theory: 2. Investigate the effects of isolator modeling approximations on vibration and structure-borne noise transmitted to a compliant receiver. The approximate isolator models, which will be examined in this article include: a. dynamic stiffness model with frequency-dependent components including coupling terms; b. spectrally-invariant stiffness model including coupling terms; c. uncoupled dynamic stiffness model with spectrally-varying components without coupling terms. These simplified isolator models along with the exact mobility model are conceptually shown in Figure 2.

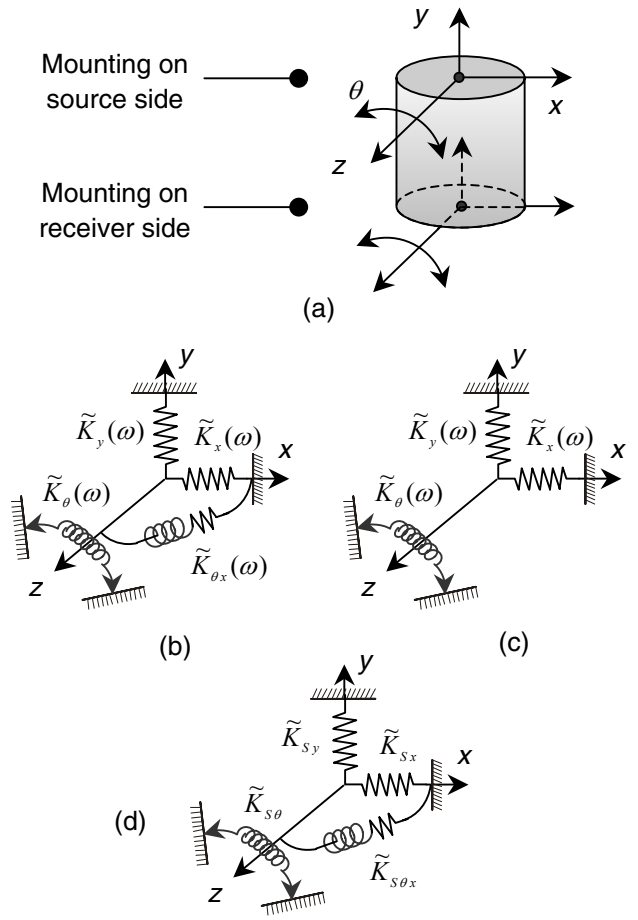

Figure 2. Multi-dimensional vibration isolator and the simplified stiffness models. (a) Mobility model ($\mathbf{K}_{\mathrm{M}}$) of a cylindrical isolator; (b) spectrally-invariant stiffness ($\mathbf{K}_{\mathrm{S}}$) model including coupling terms; (c) uncoupled dynamic stiffness ($\mathbf{K}_{\mathrm{U}}$) model with spectrally-varying components without coupling terms; (d) dynamic stiffness ($\mathbf{K}_{\mathrm{D}}$) model with frequency-dependent components including coupling terms. Here, $\widetilde{K}_y$ is the axial (longitudinal or compressional) stiffness, $\widetilde{K}_x$ is the lateral (shear) stiffness, $\widetilde{K}_\theta$ is the rotational stiffness and $\widetilde{K}_{\theta x}$ is the coupling (between lateral and rotational directions) stiffness. The $\widetilde{K}_{Sy}$, $\widetilde{K}_{Sx}$, $\widetilde{K}_{S\theta}$ and $\widetilde{K}_{S\theta x}$ are the static stiffnesses of corresponding directions. All stiffnesses are complex valued and include damping elements.

VIBRATION ISOLATOR MODELS AND THE DEVIATION INDEX

Figure 2(b-d) illustrates three alternate approximate models for a multi-dimensional isolator of Figure 2(a)

that can be completely described by the mobility model based on the continuous system theory. The mobility model $\mathbf{K}_{\mathrm{M}}$, that predicts the correct dynamic responses of an overall system, relates motions to forces at terminal locations 1 and 2 (interfacial locations with source and receiver respectively) as follows where $\mathbf{F}$ and $\mathbf{X}$ are force and displacement vectors:

$$\begin{bmatrix}\mathbf{F}_1\\ \mathbf{F}_2\end{bmatrix}=\mathbf{K}_{\mathrm{M}}\begin{bmatrix}\mathbf{X}_1\\ \mathbf{X}_2\end{bmatrix}=\begin{bmatrix}\mathbf{K}_{\mathrm{M11}}(\omega) & \mathbf{K}_{\mathrm{M12}}(\omega)\\ \mathbf{K}_{\mathrm{M21}}(\omega) & \mathbf{K}_{\mathrm{M22}}(\omega)\end{bmatrix}\begin{bmatrix}\mathbf{X}_1\\ \mathbf{X}_2\end{bmatrix}. \quad (1)$$

Here, the sub-matrices $\mathbf{K}_{\mathrm{M11}}$ and $\mathbf{K}_{\mathrm{M22}}$ are the driving point stiffness matrices, and the $\mathbf{K}_{\mathrm{M12}}$ and $\mathbf{K}_{\mathrm{M21}}$ are the transfer (cross-point) stiffness matrices. The sub-matrices are 6 by 6 for a 3-dimensional system and 3 by 3 for planer motions. Therefore, the size of a full matrix $\mathbf{K}_{\mathrm{M}}$ is 12 by 12 for a 3-dimensional motion. For example, the transfer matrix $\mathbf{K}_{\mathrm{M21}}$ of an axis-symmetric isolator in planer motions is

$$\begin{bmatrix}f_x\\ f_y\\ q_z\end{bmatrix}=\mathbf{K}_{\mathrm{M21}}\begin{bmatrix}x\\ y\\ \theta\end{bmatrix}=\begin{bmatrix}\widetilde{K}_{21,x}(\omega) & 0 & \widetilde{K}_{21,x\theta}(\omega)\\ 0 & \widetilde{K}_{21,y}(\omega) & 0\\ \widetilde{K}_{21,\theta x}(\omega) & 0 & \widetilde{K}_{21,\theta}(\omega)\end{bmatrix}\begin{bmatrix}x\\ y\\ \theta\end{bmatrix} \quad (2)$$

where $\widetilde{K}_{21,xx}$ and $\widetilde{K}_{21,\theta\theta}$ are the lateral (shear direction) and rotational stiffnesses respectively, and $\widetilde{K}_{21,x\theta}$ and $\widetilde{K}_{21,\theta x}$ are the coupling stiffnesses of the flexural motions. Further, $\widetilde{K}_{21,yy}$ is the axial (compressional) stiffness and is described here to be uncoupled from other directions for an isolator that is symmetric with respect to the y-axis. Also, f and q are force and moment, respectively. Finally, superscript ~ implies a complex quantity and such complex-valued stiffnesses incorporate the damping loss factors of an isolator.

The dynamic stiffness model $\mathbf{K}_{\mathrm{D}}$ of Figure 2(b) assumes the spatially uniform force within an isolator and is expressed as follows:

$$\begin{bmatrix}\mathbf{F}_1\\ \mathbf{F}_2\end{bmatrix}=\begin{bmatrix}-\mathbf{K}_{\mathrm{D}}(\omega) & \mathbf{K}_{\mathrm{D}}(\omega)\\ \mathbf{K}_{\mathrm{D}}(\omega) & -\mathbf{K}_{\mathrm{D}}(\omega)\end{bmatrix}\begin{bmatrix}\mathbf{X}_1\\ \mathbf{X}_2\end{bmatrix}, \quad (2)$$

$$\begin{bmatrix}f_x & f_y & q_z\end{bmatrix}^{\mathrm{T}}=\mathbf{K}_{\mathrm{D}}\begin{bmatrix}x & y & \theta\end{bmatrix}^{\mathrm{T}}=\mathbf{K}_{\mathrm{M21}}\begin{bmatrix}x & y & \theta\end{bmatrix}^{\mathrm{T}}. \quad (3)$$

Here, note that the actual forces though the isolator that can be correctly described by the mobility model are not spatially uniform and the forces at interfacial locations with source and receiver are not identical, as can be seen from (1). Therefore, the overall system behavior, which is predicted with the $\mathbf{K}_{\mathrm{D}}$ model, may deviate from the actual responses even though the dynamic stiffness model $\mathbf{K}_{\mathrm{D}}$ incorporates wave effects of mount and coupling terms.

Uncoupled dynamic stiffness model $\mathbf{K}_{\mathrm{U}}$ is also shown in Figure 2(c). The $\mathbf{K}_{\mathrm{U}}$ model is described by the following relationship:

$$\begin{bmatrix}\mathbf{F}_1\\ \mathbf{F}_2\end{bmatrix}=\mathbf{K}_{\mathrm{U}}\begin{bmatrix}\mathbf{X}_1\\ \mathbf{X}_2\end{bmatrix}=\begin{bmatrix}\mathbf{K}_{\mathrm{U11}}(\omega) & \mathbf{K}_{\mathrm{U12}}(\omega)\\ \mathbf{K}_{\mathrm{U21}}(\omega) & \mathbf{K}_{\mathrm{U22}}(\omega)\end{bmatrix}\begin{bmatrix}\mathbf{X}_1\\ \mathbf{X}_2\end{bmatrix}, \quad (4)$$

Unlike the mobility model, the $\mathbf{K}_{\mathrm{U}}$ does not include the coupling terms and consists of only the diagonal terms. For example, the sub-matrix $\mathbf{K}_{\mathrm{U21}}$ relates multi-dimensional forces to motions as follows:

$$\begin{bmatrix}f_x\\ f_y\\ q_z\end{bmatrix}=\mathbf{K}_{\mathrm{U21}}\begin{bmatrix}x\\ y\\ \theta\end{bmatrix}=\begin{bmatrix}\widetilde{K}_{21,x}(\omega) & 0 & 0\\ 0 & \widetilde{K}_{21,y}(\omega) & 0\\ 0 & 0 & \widetilde{K}_{21,\theta}(\omega)\end{bmatrix}\begin{bmatrix}x\\ y\\ \theta\end{bmatrix}. \quad (5)$$

However, the $\mathbf{K}_{\mathrm{U}}$ model is frequency-dependent and incorporates both transfer and driving point stiffnesses, like the $\mathbf{K}_{\mathrm{M}}$. Hence, only the effect of coupling stiffnesses will be examined via the $\mathbf{K}_{\mathrm{U}}$ model.

Finally, the spectrally-invariant model $\mathbf{K}_{\mathrm{S}}$ is shown in Figure 2(d). The matrix $\mathbf{K}_{\mathrm{S}}$ consists of static stiffness components including coupling terms and is described by the following where subscript S implies static stiffness:

$$\begin{bmatrix}\mathbf{F}_1\\ \mathbf{F}_2\end{bmatrix}=\begin{bmatrix}-\mathbf{K}_{\mathrm{S}} & \mathbf{K}_{\mathrm{S}}\\ \mathbf{K}_{\mathrm{S}} & -\mathbf{K}_{\mathrm{S}}\end{bmatrix}\begin{bmatrix}\mathbf{X}_1\\ \mathbf{X}_2\end{bmatrix}, \quad (6)$$

$$\begin{bmatrix}f_x\\ f_y\\ q_z\end{bmatrix}=\mathbf{K}_{\mathrm{S}}\begin{bmatrix}x\\ y\\ \theta\end{bmatrix}=\begin{bmatrix}\widetilde{K}_{Sx} & 0 & \widetilde{K}_{Sx\theta}\\ 0 & \widetilde{K}_{Sy} & 0\\ \widetilde{K}_{S\theta x} & 0 & \widetilde{K}_{S\theta}\end{bmatrix}\begin{bmatrix}x\\ y\\ \theta\end{bmatrix}. \quad (7)$$

The deviation index (Δ) of the insertion loss type (in dB) is introduced here to quantify the discrepancy of isolation performances predicted by an approximate model of an isolator with reference to an exact model.

$$\Delta_Q=10\log_{10}\left(\frac{Q_{\text{With }\mathbf{K}_{\mathrm{A}}}}{Q_{\text{With }\mathbf{K}_{\mathrm{M}}}}\right), \text{ dB.} \quad (8)$$

Here, Q is the relevant isolation or structure-borne noise measure where subscripts "with $\mathbf{K}_{\mathrm{A}}$" and "with $\mathbf{K}_{\mathrm{M}}$" represent systems with an approximate isolator model and with the exact mobility model, respectively. For example, we could employ mean-square sound pressure (ψ_p^2) or vibration power (Π_{TR}) transmitted to receiver as Q. Further, $\mathbf{K}_{\mathrm{A}}$ can be $\mathbf{K}_{\mathrm{D}}$, $\mathbf{K}_{\mathrm{U}}$ or $\mathbf{K}_{\mathrm{S}}$. Positive and negative values of Δ_Q imply over- and under- estimations of measure Q respectively by employing an approximate isolator model $\mathbf{K}_{\mathrm{A}}$.

Stiffness components of the mobility model for a rubber beam isolator with circular shape of Figure 2(a) are calculated and are shown in Figure 3. The isolator is modeled by Timoshenko beam in flexure and the wave equation for longitudinal motions and hence the effects of shear deformation and rotary inertia are incorporated. Detailed mathematical treatment is given in our earlier article [3]. The spectrally-invariant material properties and dimensions of the isolator beam are shown in Table 1. The Young's modulus E_P for a rubber material is found from the relation $E_P = 3G_P(1+QT^2)$ where Q is an empirical constant and T is the shape factor. For a circular rubber cylinder, Q is 2 and T is equal to $2r/(4L_P)$ where r and L_P are the radius and length of the isolator beam respectively [9]. Also, a frequency-invariant loss factor η_P is included in the calculation with the complex-valued Young's modulus as $\widetilde{E}_P = E_P(1+j\eta_P)$ to incorporate the hysteretic damping within the isolator.

Figure 3(a) shows that the resonances of longitudinal motion occur around at 0.7 and 1.4 kHz and the deviation between driving point and transfer stiffnesses is more pronounced at anti-resonances. Flexural stiffnesses of Figure 3(b-d) show that five distinct resonances occur from 300 to 2000 Hz. Discrepancies between driving point and transfer lateral stiffnesses increase at resonances and decrease at anti-resonances as frequency increases, as shown in Figure 3(b).

Table 1. Material properties and dimensions of source, isolator and receiver system of Figure 1.

Property or dimension	Source (Cubic rigid body)	Isolator: baseline (Circular beam)	Receiver (Rectangular plate)
m (kg)	1	-	-
E (MPa)	-	3.14	6.688 X 10^4
G (MPa)	-	1	-
η	-	0.1	0.001
ρ (kg/m^3)	-	1000	2723
Dimensions in mm	*L* = 70	*L* = 40 *r* = 12	L_a = 1000 L_b = 1000 (finite plate) *t* = 1.5 (finite or infinite plate)

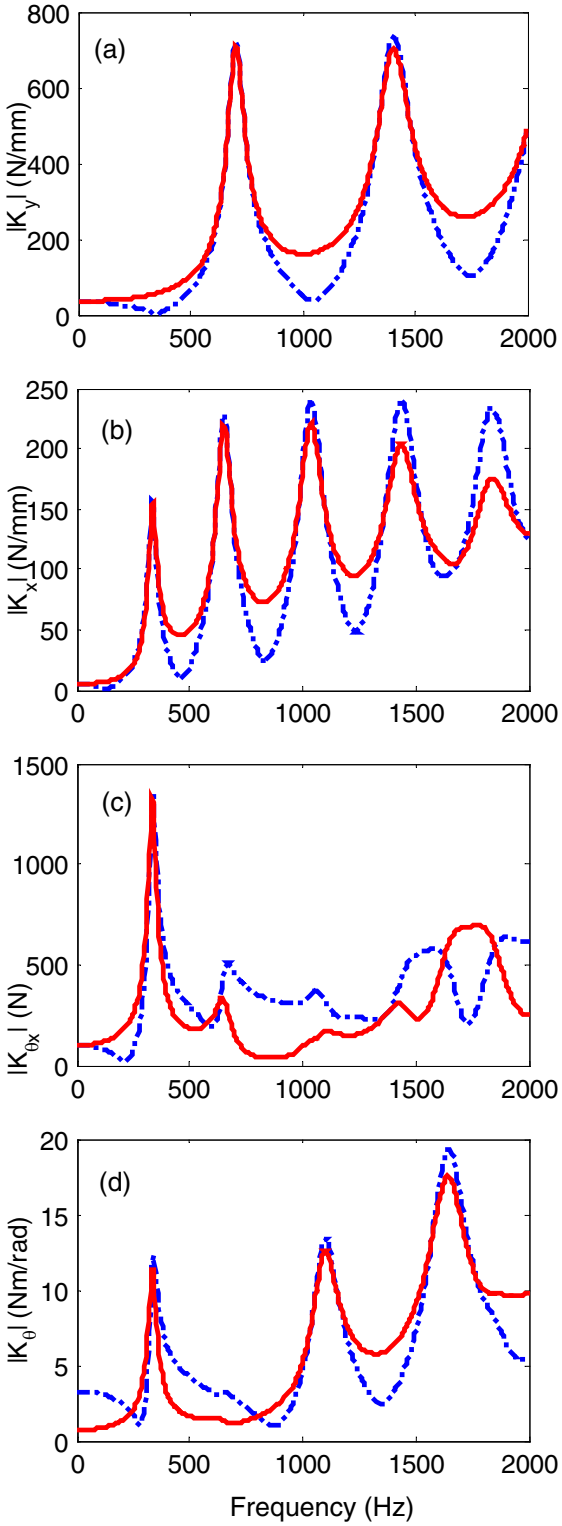

Figure 3. Dynamic stiffness components (magnitude only) of a cylindrical isolator of Figure 2(a). (a) Axial stiffness $\widetilde{K}_y$; (b) lateral stiffness $\widetilde{K}_x$; (c) coupling mobility $\widetilde{K}_{\theta x}$; (d) rotational stiffness $\widetilde{K}_\theta$. Key: —·—·— , Driving point stiffness; ——— , transfer stiffness.

Figure 3 also shows that the axial, lateral and rotational stiffnesses asymptotically increase as ω increases but the coupling stiffnesses exhibit relatively complicated spectral behavior as they simply do not increase as ω increases. Note that the flexural motions of an elastomeric isolator, that is modeled by the Timoshenko beam theory, has two different frequency response characteristics depending of frequency regime. Refer to our article for details [3]. It is further observed from Figure 3(b-d) that some resonances of rotational and coupling stiffnesses are not so distinctive as the lateral stiffness. Finally, the driving point and transfer stiffnesses for static rotational stiffness of Figure 3(d) are not identical, unlike other static stiffness components of Figure 3(a-c).

EFFECT OF ISOLATOR MODELS ON VIBRATION POWER TRANMISSION TO AN INFINITE PLATE RECEIVER

The time-averaged vibrational power (Π) is examined for an isolation system (Figure 1a) with an infinite plate receiver. Harmonic force (f_y) and moment (q_z) excitations are separately applied at the mass center of a cubic rigid body. The cylindrical isolator of Figure 2(a), with stiffnesses that have been analyzed via Figure 3, is used here. Material properties and dimensions of the receiver plate, the rigid body source and the isolator are listed in Table 1. A loss factor η_R of 0.001 is used to represent a lightly damped structure and is included in the complex-valued $\widetilde{E}_R$. The harmonic responses of the overall system are calculated by the mobility synthesis method, based on the formulation reported in our earlier article [6]. Note that the coupling mobility does not exist for an infinite plate receiver. However, a coupling arises because the motion (or force) in shear direction of an isolator is coupled with the in-plane motion of a receiver plate. Given the system properties, the effects of approximate isolator models on the total vibration power (Π_{TR}) transmitted to receiver are calculated and are shown in Figure 4. Both f_y and q_z excitation cases show that the resonances of Π_{TR} occur at the mount resonances (Figure 3) of corresponding motions, as shown in Figure 4(a). Note that the axial (with respect to isolator) Π_{TR} component dominates for f_y excitation case and flexural (lateral and rotational with respect to mount) components are dominant for q_z excitation. It is also observed from Figure 4(a) that the Π_{TR} with q_z excitation, where flexural motions of mount are dominantly involved, asymptotically decrease up to 1 kHz and increases beyond 1 kHz as frequency increases. Unlike the q_z excitation case, the f_y case where the axial motion of isolator is dominant shows that the Π_{TR} asymptotically decreases as ω increases, as shown in Figure 4(a).

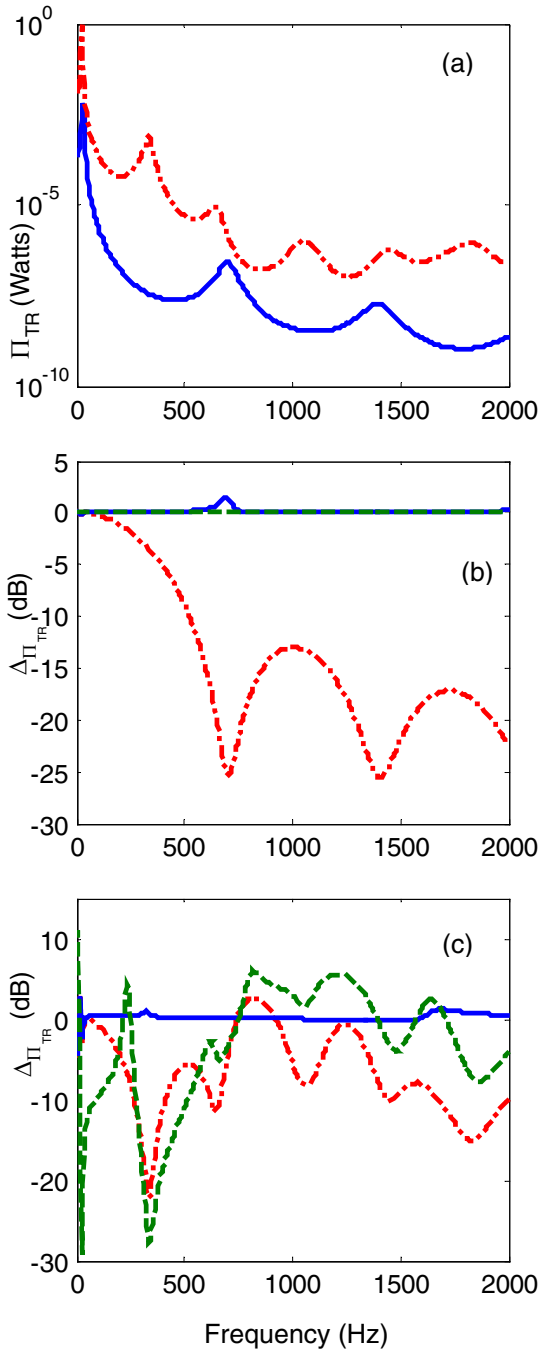

Figure 4. Vibration power (Π_{TR}) transmitted to an infinite plate receiver of Figure 1(a) and its deviation indices ($\Delta_{\Pi_{TR}}$) of isolator models. (a) Π_{TR}; Key: ——— , given force excitation; —·—·— , given moment excitation. (b) $\Delta_{\Pi_{TR}}$ given force excitation; (c) $\Delta_{\Pi_{TR}}$ given moment excitation. Key: ———, with $\mathbf{K}_D$; - - - - - - , with $\mathbf{K}_U$; —·—·— , with $\mathbf{K}_S$.

The deviation indices ($\Delta_{\Pi_{TR}}$), as defined in equation (8), of vibration power transmitted to receiver are also shown in Figures 4(b) and 4(c) for f_y and q_z excitation cases respectively. The f_y excitation case of Figure 4(b) shows that the $\Delta_{\Pi_{TR}}$ with the spectrally-invariant isolator model $\mathbf{K}_S$ is significant, especially at axial resonances of mount and its magnitudes increase as ω increases. However, the $\Delta_{\Pi_{TR}}$ with $\mathbf{K}_U$ and $\mathbf{K}_D$ models are negligible at most frequencies for f_y excitation case but $\Delta_{\Pi_{TR}}$ with $\mathbf{K}_D$ become noticeable at the first mount resonance in axial motion, as shown in Figure 4(b). For the q_z excitation case, the $\Delta_{\Pi_{TR}}$ from both $\mathbf{K}_U$ and $\mathbf{K}_S$ models are significant over a wide range of frequencies, as shown in Figure 4(c). It is also seen from Figure 4(c) that the $\Delta_{\Pi_{TR}}$ with $\mathbf{K}_D$ is less than 3 dB at most frequencies but higher than 3 dB at very low frequencies, say around 20 Hz. Figure 4(c) further shows for the q_z excitation case that the $\Delta_{\Pi_{TR}}$ from both $\mathbf{K}_U$ and $\mathbf{K}_S$ are not negative at all frequencies but their magnitudes decrease and become positive at certain frequencies, unlike the f_y excitation case. Note that the Π_{TR} with $\mathbf{K}_S$ for f_y excitation case predicts lower value than actual Π_{TR} at all frequencies, as shown in Figure 4(b). Similar to the f_y excitation case, it is observed from Figure 4(c) that the $\Delta_{\Pi_{TR}}$ magnitudes from both $\mathbf{K}_U$ and $\mathbf{K}_S$ show peaks (negative) at mount resonances of flexural motions when q_z is applied. Finally, the spectral shapes of $\Delta_{\Pi_{TR}}$ magnitudes, with $\mathbf{K}_S$ for f_y excitation and with $\mathbf{K}_U$ and $\mathbf{K}_S$ for both f_y and q_z excitations, are very similar to the ones of Π_{TR} for corresponding excitation cases.

EFFECTS OF ISOLATOR MODELS ON VIBRATIONAL BEHAVIOR OF SYSTEM WITH A FINITE PLATE RECEIVER

Similar to the infinite plate receiver, a finite plate receiver, as shown in Figure 1(b), is employed to examine the effects of mount models on the vibration power (Π_{TR}) transmitted to receiver. The isolator is connected to the finite SSSS plate at 0.75*a* and 0.5*b* where *a* and *b* are the lengths of edges. Refer to Table 1 for material properties and dimensions of the receiver plate, rigid body source and rubber isolator. Vibration power Π_{TR} and the deviation index $\Delta_{\Pi_{TR}}$ with three approximate isolator models are calculated for force (f_y) and moment (q_z) excitation cases and are shown in Figures 5 and 6, respectively.

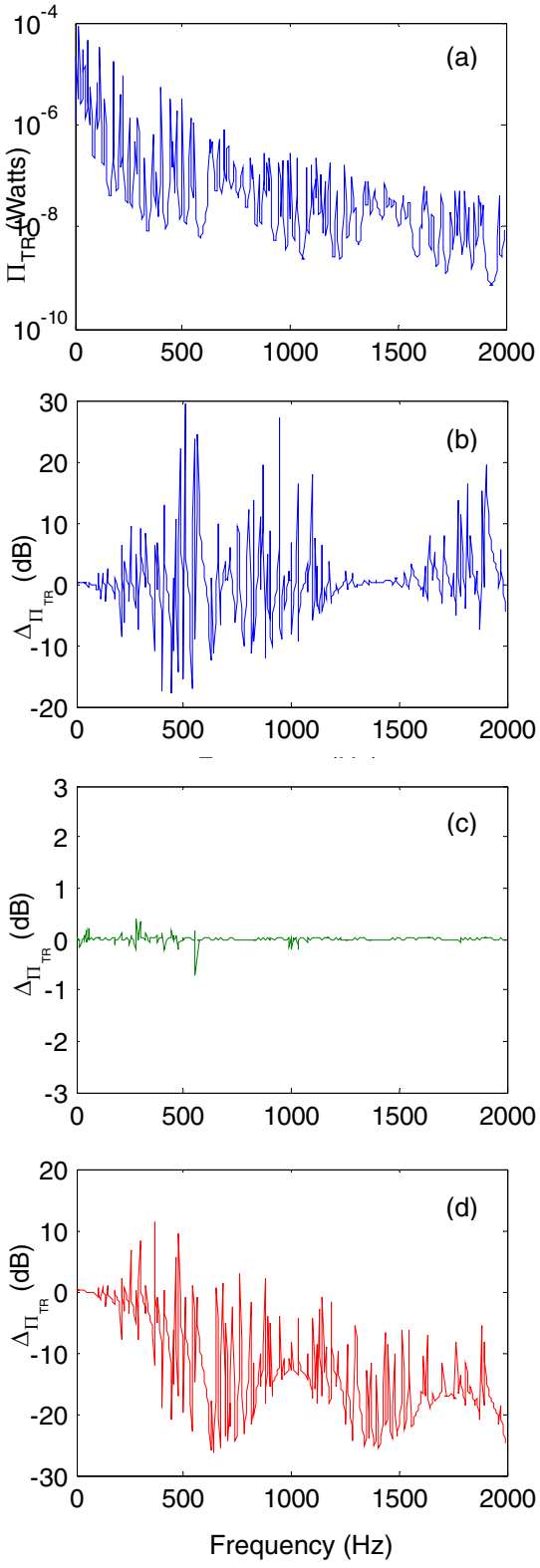

Figure 5. Vibration power (Π_{TR}) transmitted to a finite plate receiver of Figure 1(b) and its deviation indices ($\Delta_{\Pi_{TR}}$) of isolator models given force (f_y) excitation. (a) Π_{TR} with isolator of mobility model; (b) $\Delta_{\Pi_{TR}}$ with $\mathbf{K}_D$; (c) $\Delta_{\Pi_{TR}}$ with $\mathbf{K}_U$; (d) $\Delta_{\Pi_{TR}}$ with $\mathbf{K}_S$.

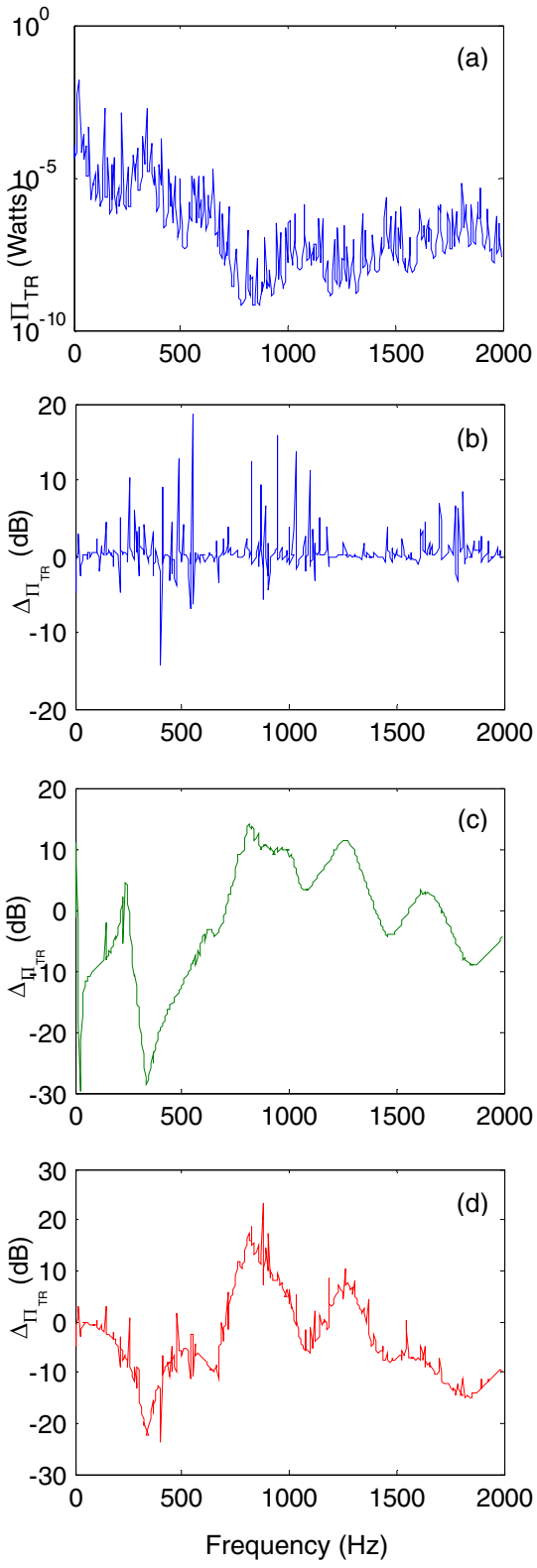

Figure 6. Vibration power (Π_{TR}) transmitted to a finite plate receiver of Figure 1(b) and its deviation indices ($\Delta_{\Pi_{TR}}$) of isolator models given moment (q_z) excitation. (a) Π_{TR} with isolator of mobility model; (b) $\Delta_{\Pi_{TR}}$ with $\mathbf{K}_{\mathrm{D}}$; (c) $\Delta_{\Pi_{TR}}$ with $\mathbf{K}_{\mathrm{U}}$; (d) $\Delta_{\Pi_{TR}}$ with $\mathbf{K}_{\mathrm{S}}$.

Figures 5 and 6 show that the asymptotic behavior of $\Delta_{\Pi_{TR}}$ with a finite plate receiver are very similar to the ones of infinite plate receiver case but the $\Delta_{\Pi_{TR}}$ is significantly contaminated by the resonances of the finite receiver plate. For example, the $\Delta_{\Pi_{TR}}$ with dynamic stiffness mode $\mathbf{K}_{\mathrm{D}}$, for both f_y and q_z excitation cases, asymptotically approach zero dB, like the infinite plate receiver case. However, the $\Delta_{\Pi_{TR}}$ with $\mathbf{K}_{\mathrm{D}}$ are considerably large (5 to 30 dB) over a wide frequency range, as shown in Figure 5(b) and 6(b). Such deviations as associated with approximate mount models arise from the mismatch of overall system resonances, especially of the receiver structure. , It is also observed from Figures 5(d) and 6(c-d) that the overall spectra of $\Delta_{\Pi_{TR}}$ fluctuate along with the spectra of mount stiffness even though the mismatched receiver resonances with high modal density are embedded to the $\Delta_{\Pi_{TR}}$. For example, the $\Delta_{\Pi_{TR}}$ with $\mathbf{K}_{\mathrm{S}}$ show asymptotic peaks (negative) at mount resonances of axial and flexural motions, as shown in Figures 5(d) and 6(d) respectively.

EFFECTS OF ISOLATOR MODELS ON STRUCTURE-BORNE NOISE TRANSMISSION TO 'L' PLATE RECEIVER

An inverted 'L' plate receiver, as shown in Figure 7, is employed to describe both in-plane and out-of plane motion transmissions to the receiver. Note that in-plane motion of the horizontal plate is coupled with flexural motion of the vertical plate and thus both plates contribute to sound radiation [8].

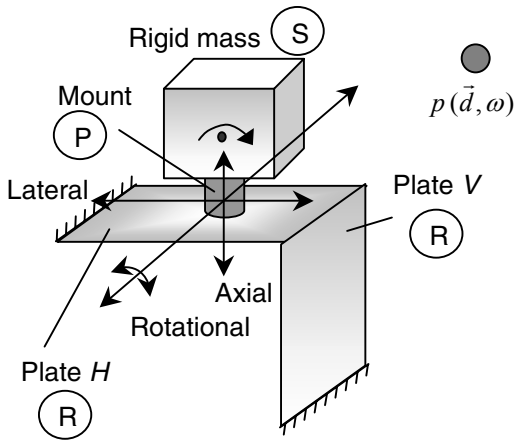

Figure 7. Structure-borne noise isolation system with an inverted 'L' plate receiver. Here, the source is modeled by a rigid body and simplified isolator models of Figure 2 describe the isolator.

The same rigid body source and rubber isolator of Table 1 are used here and, dimensions and material properties of the receiver plates along with the sound pressure location are listed in Table 2. The field point for sound pressure calculation $p(\omega)$ is located at a distance of 0.2 m from the mating edge of two plates, at 45º from the outer surfaces. The mobilities of the inverted 'L' plate structure are obtained by using a commercial finite element (FEA) IDEAS [10] code. Further, interfacial forces and moments between the isolator and receiver are calculated by synthesizing the mobilities of the inverted 'L' plate, source and isolator. Then, the plate velocity distribution from FEA calculation is provided to a commercial boundary element method (BEM) SYSNOISE [11] code to predict the sound radiation. Individual sound fields generated by each plate for interfacial forces and moments are superimposed to determine the resultant sound pressure. Note that direct radiation from either source or isolator is not included in such calculations. Overall, sound pressure amplitudes are obtained using the FEA and BEM methods. Harmonic force (f_y) and moment (q_z) are separately applied to the mass center of rigid body source.

Table 2. Material properties and dimensions of the inverted "L" plate receiver and sound pressure location of Figure 7.

Property or dimension	Inverted "L" plate receiver and acoustic free field
E (MPa)	19.5 X 10^4
η	0.001
ρ (kg/m^3)	7700
Dimensions in mm	ℓ = 400, t = 1 (Square horizontal and vertical plates)
Sound pressure location	x = 0.14, y = 0.14, z = 0

Mean-square sound pressures (Ψ_p^2) and their deviation indices ($\Delta_{\Psi_p^2}$) are calculated up to 3 kHz and are shown in Figures 8 and 9 for f_y and q_z excitation cases respectively. Results are similar to the $\Delta_{\Pi_{TR}}$ of finite plate SSSS receiver case. Asymptotic lines of $\Delta_{\Psi_p^2}$ with dynamic stiffness model $\mathbf{K}_{\mathrm{D}}$ approach zero dB and large values of $\Delta_{\Psi_p^2}$ are observed at certain frequency lines, as shown in Figure 8(b) and 9(b) for f_y and q_z excitation cases respectively. However, the large values of $\Delta_{\Psi_p^2}$ are not as much populated over frequencies as the $\Delta_{\Pi_{TR}}$ of the finite plate receiver case. Further, it is observed from Figures 8(d) and 9(c-d) that the resonances of isolator predominantly govern the overall spectral shapes of $\Delta_{\Psi_p^2}$, like the $\Delta_{\Pi_{TR}}$ of the finite plate receiver case.

Spectral averages of the deviation indices ($Savg\,\Delta_{\Psi_p^2}$) and their magnitudes ($Savg\left|\Delta_{\Psi_p^2}\right|$) are also calculated and listed in Table 3. The $Savg\left|\Delta_{\Psi_p^2}\right|$ with $\mathbf{K}_{\mathrm{S}}$ show the significant discrepancies from the exact Ψ_p^2 for both f_y and q_z excitation cases. As expected, Table 3 shows that the coupling terms can be ignored when f_y is applied but such coupling stiffnesses must be considered when q_z is applied. Further, it is also observed that the $Savg\left|\Delta_{\Psi_p^2}\right|$ with $\mathbf{K}_{\mathrm{D}}$ show relatively low values. But it appears that the error, that may be introduced by approximating the isolator with dynamic stiffness model $\mathbf{K}_{\mathrm{D}}$, is not negligible.

Furthermore, narrow band analysis may predict vastly different Ψ_p^2 when isolator is modeled by dynamic stiffness model ($\mathbf{K}_{\mathrm{D}}$), as shown in Figures 8(b) and 9(b).

Table 3. Spectral averages of the mean-square sound pressure deviation index $\Delta_{\Psi_p^2}$ for a system of Figure 7. Here, $Savg$ implies spectrally averaged value.

Isolator model	Excitation	Spectral averages of deviation index (dB)	
		$Savg\,\Delta_{\Psi_p^2}$	$Savg\left\|\Delta_{\Psi_p^2}\right\|$
$\mathbf{K}_{\mathrm{D}}$ of Figure 2(b)	Force (f_y)	0.6	1.4
	Moment (q_z)	-0.2	2.3
$\mathbf{K}_{\mathrm{U}}$ of Figure 2(c)	Force (f_y)	0	0
	Moment (q_z)	-2.7	6.5
$\mathbf{K}_{\mathrm{S}}$ of Figure 2(d)	Force (f_y)	-16.4	16.4
	Moment (q_z)	-7.7	10.2

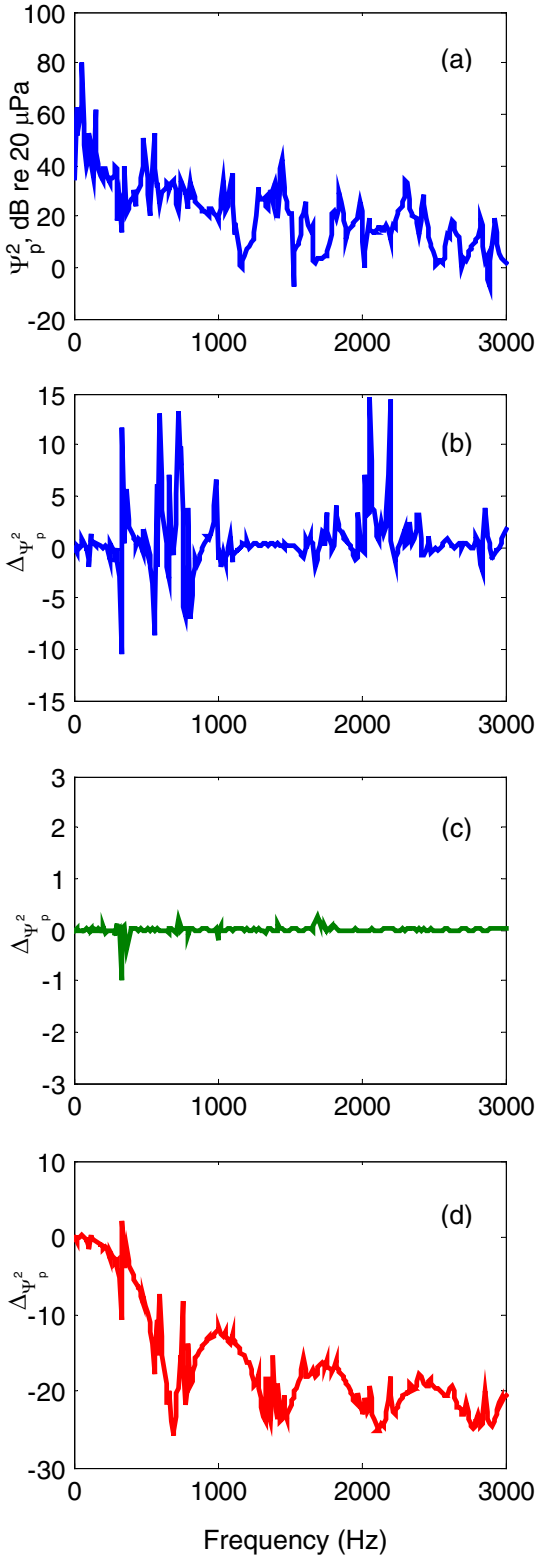

Figure 8. Mean-square sound pressure (Ψ_p^2) radiated from an inverted 'L' plate receiver of Figure 7 and its deviation indices ($\Delta_{\psi_p^2}$) of isolator models given force (f_y) excitation. (a) Π_{TR} with isolator of mobility model; (b) $\Delta_{\Pi_{TR}}$ with $\mathbf{K}_{\mathrm{D}}$; (c) $\Delta_{\Pi_{TR}}$ with $\mathbf{K}_{\mathrm{U}}$; (d) $\Delta_{\Pi_{TR}}$ with $\mathbf{K}_{\mathrm{S}}$.

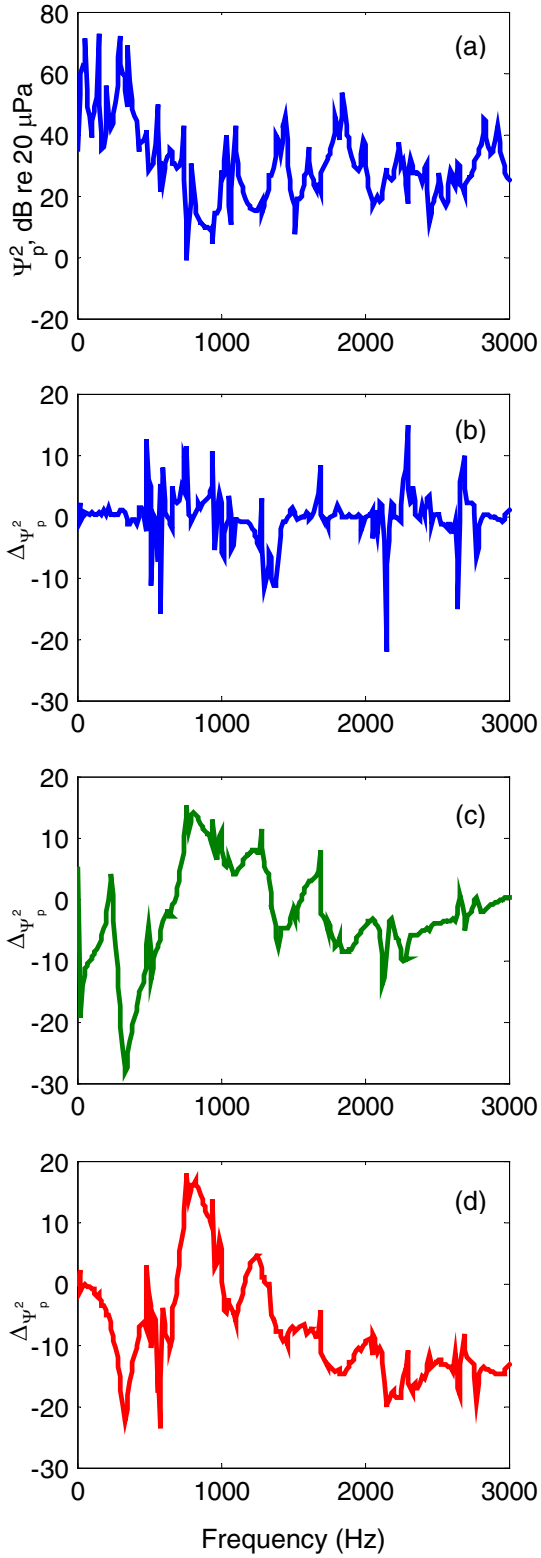

Figure 9. Mean-square sound pressure (Ψ_p^2) radiated from an inverted 'L' plate receiver of Figure 7 and its deviation indices ($\Delta_{\psi_p^2}$) of isolator models given moment (q_z) excitation. (a) Π_{TR} with isolator of mobility model; (b) $\Delta_{\Pi_{TR}}$ with $\mathbf{K}_{\mathrm{D}}$; (c) $\Delta_{\Pi_{TR}}$ with $\mathbf{K}_{\mathrm{U}}$; (d) $\Delta_{\Pi_{TR}}$ with $\mathbf{K}_{\mathrm{S}}$.

CONCLUSION

Some vibration isolator models have been examined in the context of resonant and asymptotic behaviors of a multi-dimensional vibration isolation system. Vibration power transmitted to an infinite plate or a finite plate receiver is employed as vibration isolation measure and sound radiated by an inverted 'L' plate receiver as structure-borne noise isolation measure. Those isolation measures for a system with three alternate approximate isolator models, that are commonly employed, are calculated and compared with the ones predicted for a system with an exact mobility isolator model. The approximate isolator models include spectrally-invariant stiffness, uncoupled dynamic stiffness and coupled dynamic stiffness models. Both harmonic force and moment excitation cases, where the axial and flexural motions of isolator are dominant respectively, are separately studied. Our investigation exhibits that the ignorance of frequency-dependency of isolator significantly deteriorates the prediction accuracy of sound radiation and power-based vibration measures. Further, the coupling stiffnesses of isolator are found to play a crucial role in noise and vibration transmission and hence should be incorporated in analysis when flexural motions of mount are involved. The narrow band analysis shows that the coupled dynamic stiffness model, which is frequency-dependent and assumes spatially uniform forces within isolator, also predicts considerably different vibration and noise transmissions from the exact mobility model of isolator over a wide range of frequencies. The spectrally averaged deviation index of sound radiation from the 'L' plate receiver also appears not to be negligible for the dynamic stiffness isolator model. The asymptotic behavior of the deviation spectra with spectrally-invariant stiffness and uncoupled dynamic stiffness models exhibit similar trends as the resonant behavior of mount in the corresponding motions. However, the deviation spectra with dynamic stiffness isolator model asymptotically approach zero dB even though large discrepancies due to receiver resonance mismatches are associated. Overall, the roles and effects of coupling terms, frequency dependency and discrete element modeling of a multi-dimensional isolator on vibration and sound isolation measures are identified over a broad range of frequencies. Future work is required to identify the effects of mount nonlinearity, such as preload, temperature and amplitude dependencies on vibration and noise isolation performance. Further, a reliable identification method for driving point stiffnesses needs to be developed.

ACKNOWLEDGMENTS

The General Motors Corporation (Noise and Vibration Center) and the Goodyear Tire and Rubber Company (Transportation Molded Products) are gratefully acknowledged for supporting this research.

REFERENCES

1. M. A. BERANEK 1988 *Noise and Vibration Control*. Washington, DC: Institute of Noise Control Engineering.
2. M. A. SANDERSON 1996 *Journal of Sound and Vibration*, **198**(2), 171-191. Vibration Isolation: Moments and Rotations Included.
3. S. KIM and R. SINGH 2001 *Journal of Sound and Vibration*, 248(5), 925-953. Vibration Transmission Through an Isolator Modeled by Continuous System Theory.
4. L. CREMER and M. HECKLE 1973 *Structure-Borne Sound: Structural Vibrations and Sound Radiation at Audio Frequencies*. New York: Springer-Verlag.
5. E. UNGAR and C. W. DIETRICH 1966 *Journal of Sound and Vibration*, **4**(2), 224-241. High-Frequency Vibration Isolation.
6. S. KIM and R. SINGH 2000 *Journal of Sound and Vibration*, 245(5), 877-913. Multi-Dimensional Characterization of Vibration Isolators over a Wide Range of Frequencies.
7. P. GARDONIO, S. J. ELLIOTT and R. J. PINNINGTON 1997 *Journal of Sound and Vibration*, **207**(1), 61-93. Active Isolation of Structural Vibration on a Multiple-Degree-of-Freedom System, Part I: The Dynamics of the System.
8. R. SINGH and S. KIM 2001 *Journal of Sound and Vibration*, Examination of Multi-Dimensional Vibration Isolation Measures and Their Correlation to Sound Radiation over a Broad Frequency Range (in press).
9. J. C. SNOWDON 1968 *Vibration and Shock in Damped Mechanical Systems*. New York: John Wiley & Sons.
10. I-DEAS *Users manual version 8.2.* 2000 SDRC, USA.
11. SYSNOISE Users manual version 5.4. 1999 NIT, Belgium.

LIST OF SYMBOLS

b	width
E	Young's modulus
f	force amplitude
$\mathbf{F}$	force vector
G	shear modulus
j	$\sqrt{-1}$

K	stiffness matrix
K	stiffness
L	length
m	mass
p	sound pressure
q	moment amplitude
Q	empirical constant for rubber
r	radius
S	area
Savg	spectral average
S, P, R	source, path and receiver
t	thickness
T	shape factor for rubber material
X	displacement vector
x, y, z	cartesian coordinates
Δ	deviation index
η	loss factor
θ	rotational displacement
Π	vibration power (time-averaged)
ρ	mass density
Ψ^2	mean-square
ω	frequency, rad/sec

Subscripts

D	dynamic stiffness model
M	mobility model
S	spectrally-invariant stiffness model
s	static
TR	transmitted out
U	uncoupled dynamic stiffness model
x, y, z	cartesian coordinates
θ	rotational component
1, 2	reference locations

Superscripts

~	complex valued

Operators

| |	magnitude

CONTACT

www.AutoNVH.org